TABLE III.
Treatment Details.

	With Local Recurrence, n = 17	Without Local Recurrence, n = 22	P
Energy			
^{60}Co (1.17 MV–1.33 MV)	7	3	.129
4 MV	6	13	
6 MV	4	6	
Dose per fraction, Gy			
2 (conventional fractionation)	14	15	.265
2.4 (accelerated fractionation)	3	7	
Total dose, Gy (range)			
T1 (conventional fractionation	66 (60–70)	66	.44
T1 (accelerated fractionation	60	60	
T2 (conventional fractionation	68 (60–70)	66	
T2 (accelerated fractionation)	64.8	64.8 (60–64.8)	
Wedge			
15° wedge	13	21	.297
30° wedge	1	0	
No wedge	3	1	
Bolus			
5-mm bolus	1	0	.436
No bolus	16	22	
Total treatment time, d (range)	48 (34–55)	47 (35–52)	.37
Radiation technique			
Group 1	6	9	.721
Group 2	11	13	

patients was small. Additionally, this study was a retrospective study.

This study found that expression of EpCAM might be associated with a poor radiation response, but did not reveal the mechanism underlying radiosensitivity. Future research should therefore focus on understanding the biology of EpCAM in relation to radiosensitivity.

TABLE IV.
Immunohistological Analyses.

	With Local Recurrence, n = 17	Without Local Recurrence, n = 22	P
p53			
With mutation	15	14	.083
Without mutation	2	8	
p16			
HPV-infected pattern	0	1	.564
HPV-uninfected pattern	17	21	
BerEP4			
(−)	4	15	.01*
(+)	3	6	
(++)	10	1	

*A P value <.05 was considered statistically significant.
HPV = human papillomavirus.

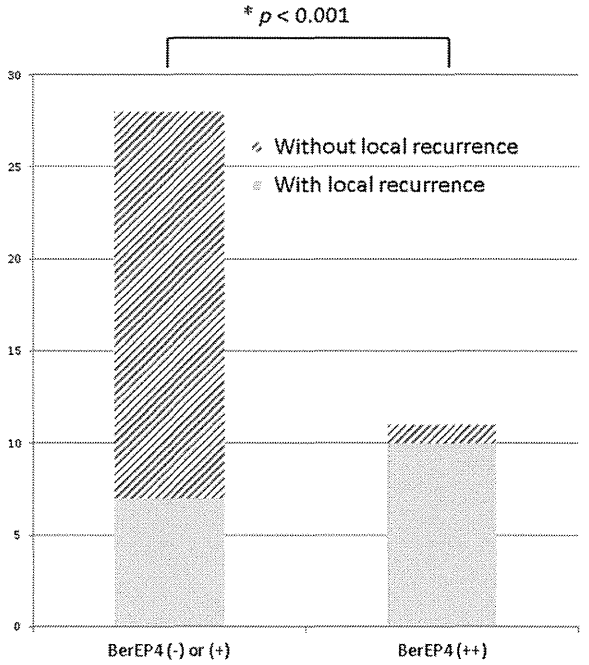

Fig. 2. Among tumors showing intense expression of BerEP4 (++), as many as 10 of 11 patients (91%) experienced local recurrence (P <.001).

CONCLUSION

A higher incidence of intense expression of EpCAM was found in HNSCCs from the hypopharynx. A strong relationship between expression of EpCAM and radiation response was demonstrated in early-stage glottic cancer. With longer follow-up, the relationship between expression of EpCAM and radiosensitivity can be investigated for HNSCC patients, especially involving the hypopharynx.

BIBLIOGRAPHY

1. Forastiere AA, Goepfert H, Maor M, et al. Concurrent chemotherapy and radiotherapy for organ preservation in advanced laryngeal cancer. *N Engl J Med* 2003;349:2091–2098.
2. Adelstein DJ, Li Y, Adams GL, et al. An intergroup phase III comparison of standard radiation therapy and two schedules of concurrent chemoradiotherapy in patients with unresectable squamous cell head and neck cancer. *J Clin Oncol* 2003;21:92–98.
3. Cooper JS, Pajak TF, Forastiere AA, et al. Postoperative concurrent radiotherapy and chemotherapy for high-risk squamous-cell carcinoma of the head and neck. *N Engl J Med* 2004;19:1937–1944.
4. Ang KK, Berkey BA, Tu X, et al. Impact of epidermal growth factor receptor expression on survival and pattern of relapse in patients with advanced head and neck carcinoma. *Cancer Res* 2002;62:7350–7356.
5. Dassonville O, Formento JL, Francoual M, et al. Expression of epidermal growth factor receptor and survival in upper aerodigestive tract cancer. *J Clin Oncol* 1993;11:1873–1878.
6. Couture C, Raybaud-Diogène H, Têtu B, et al. p53 and Ki-67 as markers of radioresistance in head and neck carcinoma. *Cancer* 2002;94:713–722.
7. Lassen P. The role of human papillomavirus in head and neck cancer and the impact on radiotherapy outcome. *Radiother Oncol* 2010;95:371–380.
8. Lindel K, Beer KT, Laissue J, Greiner RH, Aebersold DM. Human papillomavirus positive squamous cell carcinoma of the oropharynx: a radiosensitive subgroup of head and neck carcinoma. *Cancer* 2001;92:805–813.
9. Lassen P, Overgaard J, Eriksen JG. Expression of EGFR and HPV-associated p16 in oropharyngeal carcinoma: correlation and influence on prognosis after radiotherapy in the randomized DAHANCA 5 and 7 trials. *Radiother Oncol* 2013;108:489–494.
10. Okegawa T, Pong RC, Li Y, Hsieh JT. The role of cell adhesion molecule in cancer progression and its application in cancer therapy. *Acta Biochim Pol* 2004;51:445–457.

11. Trzpis M, McLaughlin PM, de Leij LM, Harmsen MC. Epithelial cell adhesion molecule: more than a carcinoma marker and adhesion molecule. *Am J Pathol* 2007;171:386–395.
12. Bellone S, Siegel ER, Cocco E, et al. Overexpression of epithelial cell adhesion molecule in primary, metastatic, and recurrent/chemotherapy-resistant epithelial ovarian cancer: implications for epithelial cell adhesion molecule-specific immunotherapy. *Int J Gynecol Cancer* 2009;19: 860–866.
13. Diaz-Arias AA, Loy TS, Bickel JT, Chapman RK. Utility of BER-EP4 in the diagnosis of adenocarcinoma in effusions: an immunocytochemical study of 232 cases. *Diagn Cytopathol* 1993;9:516–521.
14. Saadatmand S, de Kruijf EM, Sajet A, et al. Expression of cell adhesion molecules and prognosis in breast cancer. *Br J Surg* 2013;100:252–260.
15. Stoecklein NH, Siegmund A, Scheunemann P, et al. Ep-CAM expression in squamous cell carcinoma of the esophagus: a potential therapeutic target and prognostic marker. *BMC Cancer* 2006;6:165–172.
16. Imadome K, Iwakawa M, Nakawatari M, et al. Subtypes of cervical adenosquamous carcinomas classified by EpCAM expression related to radiosensitivity. *Cancer Biol Ther* 2010;10:1019–1026.
17. Barnes L, Everson JW, Reichart P, Sidransky D. *Pathology and Genetics: Head and Neck Tumors*. World Health Organization Classification of Tumours. Lyon, France: International Agency for Research on Cancer Press; 2005.
18. Patriarca C, Macchi RM, Marschner AK, Mellstedt H. Epithelial cell adhesion molecule expression (CD326) in cancer: a short review. *Cancer Treat Rev* 2012;38:68–75.
19. Nylander K, Nilsson P, Mehle C, Roos G. p53 mutations, protein expression and cell proliferation in squamous cell carcinomas of the head and neck. *Br J Cancer* 1995;71:826–830.
20. Muller PA, Vousden KH. p53 mutations in cancer. *Nat Cell Biol* 2013;15:2–8.
21. Schache AG, Liloglou T, Risk JM, et al. Evaluation of human papilloma virus diagnostic testing in oropharyngeal squamous cell carcinoma: sensitivity, specificity, and prognostic discrimination. *Clin Cancer Res* 2011; 17:6262–6271.
22. Sobin LH, Gospodarowicz MK, Wittekind C eds. *UICC: TNM Classification of Malignant Tumors*. 7th ed. New York, NY: Wiley-Liss, 2009.
23. Franchin G, Minatel E, Gobitti C, et al. Radiotherapy for patients with early-stage glottic carcinoma: univariate and multivariate analyses in a group of consecutive, unselected patients. *Cancer* 2003;98:765–772.
24. Le QT, Fu KK, Kroll S, et al. Influence of fraction size, total dose, and overall time on local control of T1-T2 glottic carcinoma. *Int J Radiat Oncol Biol Phys* 1997;39:115–126.
25. Romeu C, Farré X, Cardesa A, et al. Expression of Ep-CAM, but not of E48, associates with nodal involvement in advanced squamous cell carcinomas of the larynx. *Histopathology* 2013;62:654–961.
26. Okunieff P, Augustine E, Hicks JE, et al. Pentoxifylline in the treatment of radiation-induced fibrosis. *J Clin Oncol* 2004;22:2207–2213.

Hanaoka et al. EJNMMI Research 2014, 4:70
http://www.ejnmmires.com/content/4/1/70

EJNMMI Research
a SpringerOpen Journal

ORIGINAL RESEARCH Open Access

FBPA PET in boron neutron capture therapy for cancer: prediction of ^{10}B concentration in the tumor and normal tissue in a rat xenograft model

Kohei Hanaoka[1], Tadashi Watabe[2,3], Sadahiro Naka[4], Yasukazu Kanai[2,3], Hayato Ikeda[1], Genki Horitsugi[1], Hiroki Kato[1,3], Kayako Isohashi[1,3], Eku Shimosegawa[1,3] and Jun Hatazawa[1,3,5*]

Abstract

Background: Boron neutron capture therapy (BNCT) is a molecular radiation treatment based on the ^{10}B (n, α) ^{7}Li nuclear reaction in cancer cells, in which delivery of ^{10}B by 4-borono-phenylalanine conjugated with fructose (BPA-fr) to the cancer cells is of critical importance. The PET tracer 4-borono-2-^{18}F-fluoro-phenylalanine (FBPA) has been used to predict the accumulation of BPA-fr before BNCT. However, because of the difference in chemical structure between BPA-fr and FBPA and the difference in the dose administered between BPA-fr (therapeutic dose) and FBPA (tracer dose), the predictive value of FBPA PET for BPA-fr accumulation in the tumor and normal tissues is not yet clearly proven. We conducted this study to validate FBPA PET as a useful test to predict the accumulation of BPA-fr in the tumor and normal tissues before BNCT.

Methods: RGC-6 rat glioma cells (1.9×10^7) were implanted subcutaneously in seven male F344 rats. On day 20 after the tumor implantation, dynamic PET scan was performed on four rats after injection of FBPA for 1 h. Whole-body PET/CT was performed 1 h after intravenous injection of the FBPA solution (30.5 ± 0.7 MBq, 1.69 ± 1.21 mg/kg). PET accumulation of FBPA in the tumor tissue and various normal tissues was estimated as a percentage of the injected dose per gram (%ID/g). One hour after the PET/CT scan, BPA-fructose (167.32 ± 18.65 mg/kg) was injected intravenously, and the rats were dissected 1 h after the BPA-fr injection. The absolute concentration of ^{10}B in the autopsied tissues and blood was measured by inductively coupled plasma optical emission spectrometry (ICP-OES).

Results: The highest absolute concentration of ^{10}B determined by ICP-OES was found in the kidney (4.34 ± 0.84 %ID/g), followed by the pancreas (2.73 ± 0.63 %ID/g), and the tumor (1.44 ± 0.44 %ID/g). A significant positive correlation was found between the accumulation levels of BPA-fr and FBPA ($r = 0.91$, $p < 0.05$).

Conclusions: FBPA PET can reliably predict accumulation of BPA-fr in the tumor as well as normal tissues.

Keywords: Boron nuclear capture therapy; Boron concentration; FBPA; BPA-fr

Background

Boron neutron capture therapy (BNCT) is based on the nuclear capture reaction of ^{10}B (n, α) ^{7}Li by low-energy neutrons produced by a nuclear reactor or more recently accelerator. High-energy α particles and lithium ions have been shown to exert a cell-killing effect. In the presence of ^{10}B specifically in cancer cells, these particles have been demonstrated to exert a cancer-cell-specific killing effect, because of the short track ranges of these particles (9 to 10 μm for α particles and 4 to 5 μm for ^{7}Li nuclei) [1-3]. In BNCT, the requisite concentration of ^{10}B in the tumor has been estimated to be 15 ppm or more [2]. It is also important to estimate the ^{10}B concentration in normal tissues/organs to avoid radiation injury to normal tissues [4-6].

In the present BNCT practice, L-paraboronophenylalanine labeled with ^{10}B and conjugated with fructose (BPA-fr) is mainly used as the carrier of ^{10}B into the

* Correspondence: hatazawa@tracer.med.osaka-u.ac.jp
[1]Department of Nuclear Medicine and Tracer Kinetics, Osaka University Graduate School of Medicine, Suita, Japan
[3]PET Molecular Imaging Center, Osaka University Graduate School of Medicine, Suita, Japan
Full list of author information is available at the end of the article

tumor cells. In order to evaluate BPA-fr accumulation in the tumors, 4-borono-2-^{18}F-fluoro-phenylalanine (FBPA) PET has been employed [4]. Imahori et al. demonstrated that both BPA-fr and FBPA accumulated in high concentration in high-grade gliomas [5]. In clinical practice, the measurement of FBPA accumulation was made about 1 h after FBPA administration [7-10]. However, there are several limitations of FBPA PET in predicting BPA-fr accumulation in the tumors and normal tissues. Firstly, the chemical structure of FBPA differs from that of BPA-fr. Secondly, FBPA PET provides tracer-dose pharmacokinetics of FBPA, while therapeutic doses of ^{10}BPA are administered (approximately 500 mg/kg) for BNCT. Thirdly, BPA-fr is administered by slow bolus intravenous injection followed by drip infusion during neutron irradiation, while FBPA is administered by a single bolus injection. Because of these differences, the predictive value of FBPA PET for BPA-fr accumulation in the tumor and normal tissues remains unclear.

In the preset experiment, we first measured the radioactivity accumulation in transplanted tumors and normal organs in rats by means of PET/CT carried out after administration of a tracer dose of FBPA. We then administered a therapeutic dose of BPA-fr and quantified the absolute concentration of ^{10}B in autopsy specimens by means of inductively coupled plasma optical emission spectrometry (ICP-OES). The correlations between the ^{10}B concentrations after BPA-fr injection and the uptake values of FBPA in FBPA PET were examined in the tumors and normal organs.

Methods

Synthesis of L-[^{18}F] FBPA

FBPA was prepared as described previously [4], although with several modifications, using an F-1 synthesizer (Sumitomo Heavy Industries, Tokyo, Japan). In brief, ^{18}F-acetylhypofluorite was bubbled at a flow rate of 600 mL/min at room temperature into 5 mL of trifluoroacetic acid containing 30 mg of 4-borono-L-phenylalanine. Next, trifluoroacetic acid was removed by passing N_2 under reduced pressure at a flow rate of 200 mL/min. The residue was dissolved in 3 mL of 0.1% acetic acid, and the solution was applied to YMC-Pack ODS-A, a high-performance liquid chromatography column (20 mm in inner diameter × 150 mm in length; YMC, Kyoto, Japan), under the following conditions: mobile phase, 0.1% acetic acid; flow rate, 10 mL/min; ultraviolet detector at 280 nm; and radioactivity detector. The FBPA fraction (retention time = 19 to 21 min) was collected. After drying of the FBPA fraction, the residue was dissolved in saline. The radiochemical purity of FBPA was >98%, and the specific activity at the end of the synthesis was 49.7 ± 17.3 GBq/mmol as determined by HPLC.

Preparation of the BPA-fructose complex

BPA was solubilized at neutral pH for intravenous infusion by allowing it to form a complex with fructose. Injection solutions of the BPA-fructose complex (BPA-fr) were prepared at a concentration of 10 mg BPA/0.43 mL using a previously published procedure with modifications [6].

Glioma tumor model preparation

Seven male F344/NJcl-rnu/rnu rats (11 to 13 weeks; 241.7 ± 28.0 g) obtained from CLEA Japan (Tokyo, Japan) were used for this study. The RGC-6 rat glioma cell was obtained from RIKEN BRC (Tsukuba, Japan) through the National Bio-Resource Project of MEXT, Japan. RGC-6 cells (1.9×10^7) were implanted subcutaneously as a cell/Matrigel mixture into the backs of F344 rats. On day 20 after the tumor implantation, the rats were starved for 8 h. The animal studies were conducted with the approval of the Animal Care and Use Committee of Osaka University.

FBPA PET/CT procedure

Rats anesthetized by inhaled 2% isoflurane plus 100% oxygen at 2 L/min were intravenously injected with FBPA at a dose of 30.5 ± 0.7 MBq (1.69 ± 1.21 mg/kg body weight) [11]. To minimize the influence of BPA-fr accumulation from FBPA, the dose of FBPA was set as tracer dose. Then, the rats were imaged with micro PET/CT (Inveon; Siemens Medical Solutions, Knoxville, TN, USA) in a prone position. In four of seven rats, dynamic images were obtained during 1 h (30 frames of 2 min) after the injection. To measure FBPA in comparison with BPA-fr quantification, static images were obtained in seven rats 1 h after the injection for 10 min (5 min/per bed position, two bed positions). All PET images were reconstructed by 2D ordered-subset expectation maximization (16 subsets, 4 iterations) with a 128 × 128 pixel image matrix. The spatial resolution at the center of the field of view (FOV) was 1.62 mm [12]. The CT images were acquired at a tube voltage of 80 kVp and tube current of 140 μA for scatter and attenuation correction. The injected radioactivity of FBPA was measured by a well-type scintillation counter (BeWell; Molecular Imaging Labo, Osaka, Japan). Regions of interest (ROIs) were placed over the tumor, brain, lung, liver, spleen, pancreas, small intestine, large intestine, kidney, and blood pool in the left ventricle on the decay-corrected PET images with reference to CT images. The maximum and average counts in the voxel were automatically converted to radioactivity per milliliter (Bq/mL) by the cross-calibration factor in the PET reconstruction process. Time-activity curves were plotted for both the tumor and the normal tissues, excluding the spleen and intestine. Based on the assumption that tissue density is 1 g/mL, values were converted to radioactivity per gram of tissue (Bq/g). The percentage of the injected dose per

gram of tissue (%ID/g) was determined by dividing the radioactivity per gram (Bq/g) by the injected amount of radioactivity (Bq).

^{10}B assay in RGC-6 glioma-bearing F344 rats after BPA-fr injection

One hour after the PET/CT scan, 40 mg BPA-fr (167.32 ± 18.65 BPA mg/kg body weight) was injected bolus through the tail vein of each rat. The rats were sacrificed 1 h after the BPA-fr injection, and the following tissue samples were collected: tumor, brain, lung, liver, spleen, pancreas, small intestine, large intestine, kidney, and blood. The absolute ^{10}B concentrations in the tissue samples were measured by ICP-OES (Vista-MPX ICP-OES spectrometer, Seiko Instruments, Chiba, Japan) [13,14]. The concentrations of ^{10}B from BPA-fr in the normal tissues and tumor tissues were normalized to %ID/g. A part of the tumor tissue was stained with hematoxylin and eosin for light microscopy examination.

Data analysis

The concentrations of FBPA and BPA-fr in the tissues, which were measured by PET/CT and ICP-OES, respectively, were shown as mean ± SD. The Pearson product-moment correction coefficients were calculated to evaluate the correlations between the FBPA accumulations measured by PET/CT and BPA-fr accumulations measured by ICP-OES. Wilcoxon's signed-rank test was performed to compare the accumulation level of FBPA estimated by PET/CT and accumulation level of BPA-fr measured by ICP-OES in each of the tissues. All the statistical analyses were performed with the SPSS software (Version 17, SPSS Inc., Chicago, IL, USA), and a p value of less than 0.05 indicated a significant difference.

Results

Table 1 shows absolute values of boron concentrations measured by ICP-OES in the tissues. The highest concentration was found in the kidney, followed by that in the pancreas and the glioma tumor tissue.

Figure 1 shows the time-activity curves based on average count of the tumor and several organs in F344 rats after administration of FBPA. Time-activity curves of the tumor and normal tissues showed various patterns of rapidly increasing FBPA uptake up to 20 min, which stabilized or decreased thereafter gradually. Dynamic PET data demonstrated the ratio of tumor to blood (1.24, 1.67, and 1.71) at 10, 30, and 60 min after administration of FBPA, respectively.

The accumulation levels of FBPA measured by PET/CT and expressed as %ID/g demonstrated significant positive correlations with the accumulation levels of BPA-fr measured by ICP-OES and expressed as %ID/g; the regression lines were as follows: $y = 1.21x - 0.31$ ($r = 0.92$, $p < 0.05$) for FBPA accumulation based on the maximum count and $y = 0.97x - 0.34$ ($r = 0.91$, $p < 0.05$) for FBPA accumulation based on the average count (Figures 2 and 3).

Table 1 Absolute of boron concentration after injection of 40 mg (167.32 ± 18.65 mg/kg body weight) BPA by ICP-OES (ppm)

	Absolute of boron concentration (ppm)	
	Median	Mean ± SD
Tumor	24.31	27.56 ± 8.42
Brain	7.73	7.66 ± 1.15
Lung	17.76	15.12 ± 3.83
Liver	13.80	14.93 ± 2.49
Spleen	19.04	20.48 ± 4.59
Pancreas	50.66	52.25 ± 12.06
Small intestine	16.45	16.46 ± 2.49
Large intestine	12.97	13.21 ± 1.53
Kidney	77.64	83.06 ± 16.08
Blood	12.44	12.25 ± 0.96

Figure 4 depicts the FBPA PET/CT images of a RGC-6 glioma-bearing F344 rat. Significant accumulation in the tumor and high radioactivity contrast between the tumor and normal tissues are observed. High uptakes of FBPA in the kidneys and pancreas of the rats are seen.

Table 2 shows the accumulation levels of FBPA measured by PET/CT and accumulation levels of BPA-fr measured by ICP-OES, expressed as %ID/g of tissue. The estimated values by FBPA PET based on the maximum count in the blood, brain, liver, pancreas, and tumor were similar to the values measured by ICP-OES. The differences did not exceed 15% in any of these tissues. In the lung, small intestine, and large intestine, the FBPA accumulation measured by FBPA PET based on the maximum count and average count was significantly underestimated. In the tumor, the value based on the average count was significantly underestimated. In the kidney, the value based on the maximum count was significantly overestimated.

Figure 5 shows a light microscopy image of a hematoxylin-eosin-stained section (scale bars = 100 μm) of the glioma, showing the heterogeneity of the lesion.

Discussion

In this study, we demonstrated a significant correlation between the concentrations of ^{10}B and accumulation levels of FBPA in tumors and various normal organs, despite the differences in the chemical structure and dose administered between BPA-fr and FBPA.

Kabalka et al. reported the optimal time for neutron exposure after infusion of BPA-fr. They reported that the tumor-to-blood activity ratio of humans appeared to plateau after 60 mm [10]. In the present study, the time

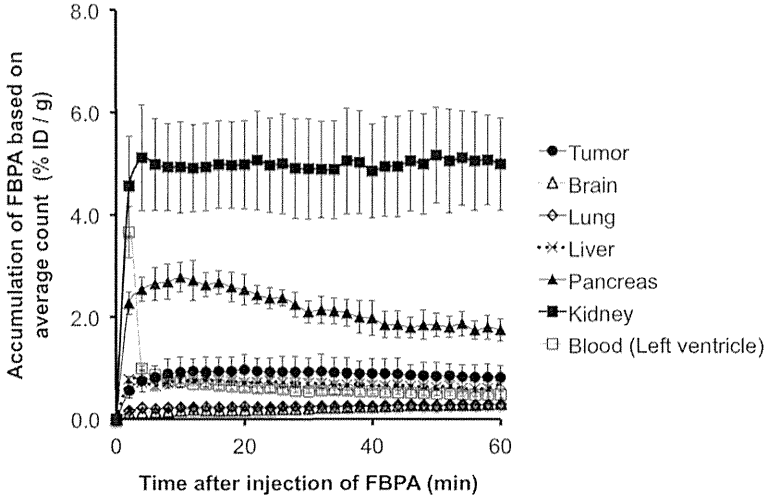

Figure 1 Time-activity curve. Based on average count of tumor and normal organs in F344 rats after administration of FBPA.

point of 1 h after administration for FBPA PET may be considered appropriate because the tumor-to-blood ratio becomes stable. More time points are needed for in-depth dosimetric studies. Nevertheless, one time point of 1 h is a good compromise to obtain a quantitative value that can be correlated with other variables.

Yoshimoto et al. recently reported that FBPA is predominantly transported via the L-type amino acid transporter in human glioblastoma cells [15]. They also demonstrated that uptake of FBPA into human glioblastoma cells was inhibited by high concentrations of BPA in the medium, suggesting that FBPA and BPA share the same transporter system. Imahori et al. also reported that the ^{10}B concentrations in surgically removed specimens of glioblastoma after administration of BPA-fr at therapeutic doses were predicted by using the rate constants of FBPA PET [16].

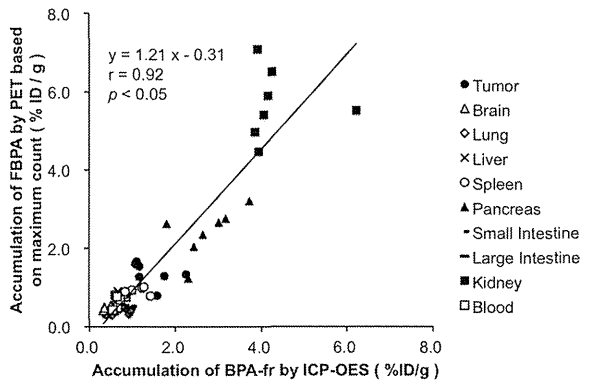

Figure 2 Correlation between accumulation levels based on maximum count. Correlation between the accumulation level of BPA-fr measured by ICP-OES and that of FBPA estimated by FBPA PET/CT based on the maximum count in a rat model.

In this study, the injected dose of BPA-fr was about 100 times higher than that of FBPA. Notwithstanding, significant correlations were observed between the amounts of BPA-fr and FBPA accumulated in the tumors as well as normal organs. Our results suggest that FBPA PET can be used to estimate the amount of BPA accumulation in the normal surrounding tissues during BNCT. The accumulation levels of both BPA and FBPA in the pancreas were remarkably high (2.73 and 2.42 %ID/g, respectively). This finding suggests that radiation injury of the pancreas should be anticipated when BNCT is employed for abdominal cancers.

There are several reports suggesting similar pharmacokinetics between BPA-fr and FBPA in normal tissues/organs. Wang et al. [17] measured the radioactivity in glioma and normal tissues after injection of FBPA-fr by a γ-scintillation counter and compared the ^{10}B concentrations by ICP-MS after injection of BPA-fr as the tumor-to-normal tissue ratio. The tumor-to-normal tissue uptake ratio of FBPA-fr was parallel to that of BPA-fr. Yang et al. [18,19] reported the pharmacokinetic analysis of FBPA and BPA-fr after ultrasound-induced blood-brain barrier disruption. Ishiwata et al. [20] reported that the ratios of the concentrations of FBPA to those of BPA in the tumor, blood, and muscle measured by a NaI(Tl) gamma counter and ICP-AES, respectively, ranged from 0.70 to 1.00. These reports lend support to our view that FBPA PET can be used for the assessment of BPA accumulation in normal tissues/organs during BNCT in an attempt to avoid radiation injury.

In BNCT, the subcellular location of ^{10}B is of critical importance for the cell-killing effect, because the trace ranges of α particles and ^{7}Li are very short. Chandra et al. [21] reported that there was no significant difference in the intracellular distribution between FBPA and BPA as

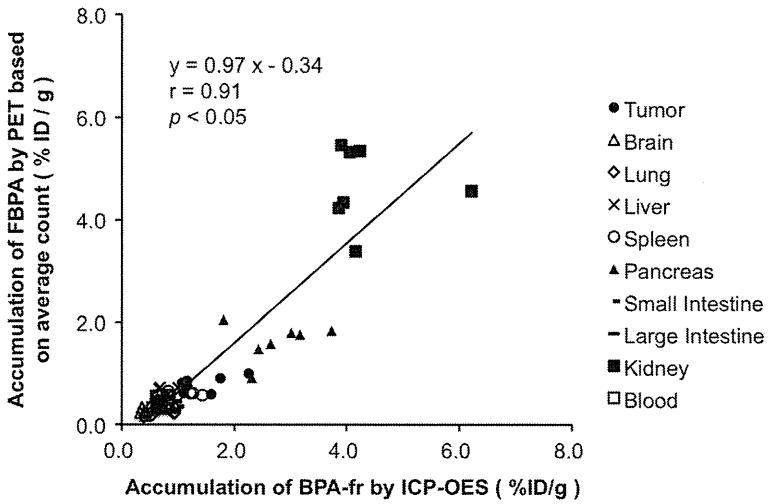

Figure 3 Correlation between accumulation levels based on average count. Correlation between the accumulation level of BPA-fr measured by ICP-OES and that of FBPA estimated by FBPA PET/CT based on the average count in a rat model.

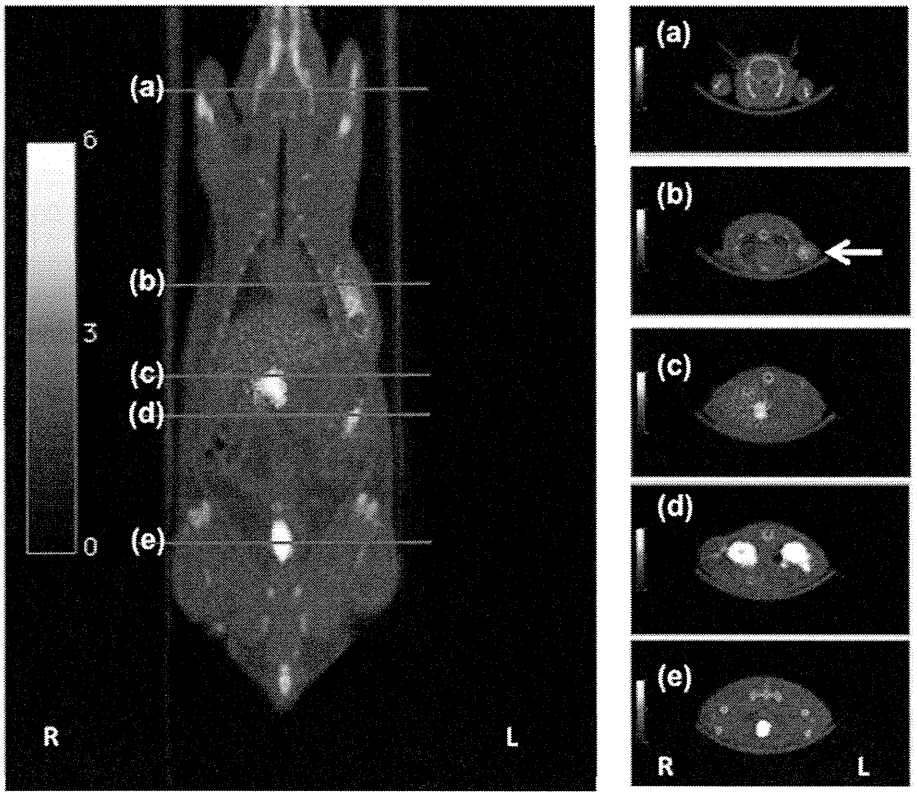

Figure 4 PET/CT images of a RGC-6 glioma-bearing F344 rat. PET/CT fused images of F344 male rats with RGC-6 glioma xenografts 60 min after injection of approximately 30 MBq of FBPA. **(a)** At the level of brain, **(b)** at the level of heart and transplanted tumor, **(c)** at the level of pancreas and liver, **(d)** at the level of kidneys, and **(e)** at the level of bladder (all transaxial images). FBPA accumulation in the tumor was found in the plane **(b)** indicated by an arrow. In the planes **(c)**, **(d)**, and **(e)**, high accumulations were found in the pancreas, kidneys, and bladder, respectively.

Table 2 Biodistribution of BPA-fr and [^{18}F] FBPA in various organs of RGC6 glioma-bearing Fischer 344 rats ($n = 7$)

	Accumulation of BPA-fr by ICP-OES (%ID/g)		Accumulation of FBPA by PET based on maximum count (%ID/g)		Accumulation of FBPA by PET based on average count (%ID/g)	
	Median	Mean ± SD	Median	Mean ± SD	Median	Mean ± SD
Tumor	1.27	1.44 ± 0.44	1.34	1.36 ± 0.31	0.80	0.79 ± 0.18*
Brain	0.40	0.40 ± 0.06	0.41	0.43 ± 0.07	0.26	0.27 ± 0.07*
Lung	0.93	0.79 ± 0.20	0.39	0.38 ± 0.05*	0.23	0.25 ± 0.05*
Liver	0.72	0.78 ± 0.13	0.78	0.78 ± 0.14	0.59	0.61 ± 0.12
Spleen	0.99	1.07 ± 0.24	0.89	0.88 ± 0.10	0.59	0.58 ± 0.08*
Pancreas	2.65	2.73 ± 0.63	2.64	2.42 ± 0.63	1.76	1.63 ± 0.36*
Small intestine	0.86	0.86 ± 0.13	0.48	0.52 ± 0.10*	0.36	0.36 ± 0.08*
Large intestine	0.68	0.69 ± 0.08	0.44	0.46 ± 0.09*	0.30	0.30 ± 0.07
Kidney	4.06	4.34 ± 0.84	5.52	5.70 ± 0.89*	4.56	4.66 ± 0.76
Blood	0.65	0.64 ± 0.05	0.59	0.61 ± 0.14	0.45	0.47 ± 0.10*

*$p < 0.05$ compared to BPA-fr by ICP-OES.

assessed by ion microscopy. Therefore, it is expected that FBPA PET would reflect the intracellular distribution of BPA-fr and predict the therapeutic effect of α particles and ^{7}Li which have short track ranges.

In our study, underestimations by FBPA PET were observed in the lung and intestines. One of the reasons for this may be the partial volume effect, because of the limit of resolution of PET. The partial volume effect, which occurs at sizes less than or equal to three times the full width at half maximum, was not corrected for this study [22,23]. The full width at half maximum of the PET system used in this study in axial resolutions at the center of the FOV was 1.62 mm; therefore, differences in the sizes of the tissues may influence the %ID/g. Especially in the lung and intestines, the influence of the partial volume effect is serious, because the regions of interest on the PET images contain air [24].

On the other hand, overestimation was noted in the kidney. FBPA is metabolically stable. During the initial 1 h, about half of the injected amount of tracer was passed into the urine [25]. In the kidney, contamination with the count from the urine contained in the ureter or renal pelvis should be considered on FBPA PET images.

In the tumor, there was a 40% difference between the maximum count and average count on FBPA PET images. The slight overestimation of the accumulation level in the tumor in this study is mainly because gliomas consist of heterogeneous tissue components, including viable portions, central necrosis areas, and peritumoral infiltration areas [26] (Figure 5).

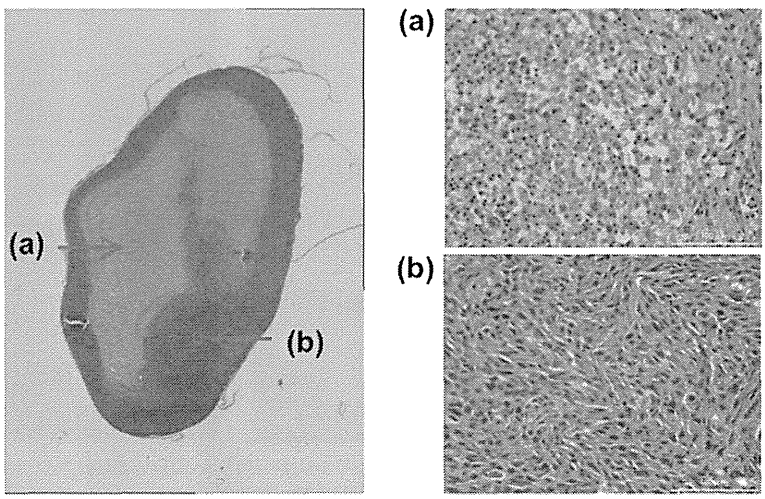

Figure 5 Representative light microscopy images of the glioma (hematoxylin-eosin staining). Area **(a)** has a lower cell density than area **(b)**, indicating the heterogeneity of the tumor components.

Conventionally, BNCT has been used for the medical treatment of malignant melanoma [27], malignant brain tumors [5,16,28-30], and cancer of the neck [31]. In recent years, adoption of BNCT has expanded to liver cancer [32], breast cancer, and lung cancer [33]. Therefore, prediction of the absolute concentration of BPA in the normal tissues in individual patients is very important to minimize the radiotoxicity to normal healthy tissues during BNCT.

Our study had some limitations. First, the method of administration of BPA-fr for BNCT is different from the infusion method adopted for administration of FBPA for PET/CT, especially because PET examination requires only a low dose of FBPA. BPA is administered via intravenous infusion. Therefore, determination of the offset according to the infusion method of BPA-fr is required to ensure the accuracy of the clinical data.

Second, the biodistribution of FBPA in animals differs from that in humans [25]. Especially in the pancreas, the expression levels of LAT1 between rats and humans are different. The accumulation levels of FBPA and BPA-fr determined in this research may therefore not be applicable to clinical cases. Further clinical FBPA PET study is required to determine BPA-fr distribution in the cancer patients.

Conclusions

In this study, we demonstrated the existence of clear correlations between the accumulation levels of BPA-fr and FBPA in the transplanted glioma cells and normal organs in rat xenograft models. This preclinical study indicates the validity of FBPA PET for predicting BPA-fr accumulation in tumors and normal tissues/organs in BNCT. Further studies are required to estimate the ^{10}B concentrations in tissues following BPA-fr administration according to a clinical protocol, such as slow infusion and drip infusion of BPA during neutron irradiation.

Competing interests

The authors declare that they have no competing interests.

Authors' contributions

KH, TW, ES, and JH participated in the design of the study and performed the statistical analysis. Data acquisition was done by KH, TW, SN, YK, HI, and GH. Data analysis was done by KH, KI, HK, and TW. The manuscript was prepared by KH. All authors read and approved the final manuscript.

Acknowledgements

This study was supported by the KAKENHI Grant-in-Aid for Scientific Research (S) (No. 24229008) and Molecular Imaging Research Strategic Program, and Grant (No. 10048012 and No. 24591758) from the Ministry of Education, Culture, Sports, Science and Technology, Japan.

Author details

[1]Department of Nuclear Medicine and Tracer Kinetics, Osaka University Graduate School of Medicine, Suita, Japan. [2]Department of Molecular Imaging in Medicine, Osaka University Graduate School of Medicine, Suita, Japan. [3]PET Molecular Imaging Center, Osaka University Graduate School of Medicine, Suita, Japan. [4]Osaka University Hospital, Suita, Japan. [5]Immunology Frontier Research Center, Osaka University, Suita, Japan.

Received: 17 October 2014 Accepted: 27 November 2014
Published online: 20 December 2014

References

1. Evangelista L, Jori G, Martini D, Sotti G: **Boron neutron capture therapy and 18F-labelled borophenylalanine positron emission tomography: a critical and clinical overview of the literature.** *Appl Radiat Isot* 2013, **74**:91–101. doi:10.1016/j.apradiso.2013.01.001.
2. Pisarev MA, Dagrosa MA, Juvenal GJ: **Boron neutron capture therapy in cancer: past, present and future.** *Arq Bras Endocrinol Metabol* 2007, **51**(5):852–856.
3. Wittig A, Michel J, Moss RL, Stecher-Rasmussen F, Arlinghaus HF, Bendel P, Mauri PL, Altieri S, Hilger R, Salvadori PA, Menichetti L, Zamenhof R, Sauerwein WA: **Boron analysis and boron imaging in biological materials for boron neutron capture therapy (BNCT).** *Crit Rev Oncol Hematol* 2008, **68**(1):66–90. doi:10.1016/j.critrevonc.2008.03.004.
4. Ishiwata K, Ido T, Mejia AA, Ichihashi M, Mishima Y: **Synthesis and radiation dosimetry of 4-borono-2-[18F]fluoro-D, L-phenylalanine: a target compound for PET and boron neutron capture therapy.** *Int J Rad Appl Instrum A* 1991, **42**(4):325–328.
5. Imahori Y, Ueda S, Ohmori Y, Kusuki T, Ono K, Fujii R, Ido T: **Fluorine-18-labeled fluoroboronophenylalanine PET in patients with glioma.** *J Nucl Med* 1998, **39**(2):325–333.
6. Yoshino K, Suzuki A, Mori Y, Kakihana H, Honda C, Mishima Y, Kobayashi T, Kanda K: **Improvement of solubility of p-boronophenylalanine by complex formation with monosaccharides.** *Strahlenther Onkol* 1989, **165**(2–3):127–129.
7. Wang LW, Wang SJ, Chu PY, Ho CY, Jiang SH, Liu YW, Liu YH, Liu HM, Peir JJ, Chou FI, Yen SH, Lee YL, Chang CW, Liu CS, Chen YW, Ono K: **BNCT for locally recurrent head and neck cancer: preliminary clinical experience from a phase I/II trial at Tsing Hua Open-Pool Reactor.** *Appl Radiat Isot* 2011, **69**(12):1803–1806. doi:10.1016/j.apradiso.2011.03.008.
8. Aihara T, Hiratsuka J, Morita N, Uno M, Sakurai Y, Maruhashi A, Ono K, Harada T: **First clinical case of boron neutron capture therapy for head and neck malignancies using 18 F-BPA PET.** *Head Neck* 2006, **28**(9):850–855. doi:10.1002/hed.20418.
9. Ariyoshi Y, Shimahara M, Kimura Y, Ito Y, Shimahara T, Miyatake SI, Kawabata S: **Fluorine-18-labeled boronophenylalanine positron emission tomography for oral cancers: qualitative and quantitative analyses of malignant tumors and normal structures in oral and maxillofacial regions.** *Oncology Letters* 2011, **2**(3):423–427. doi:10.3892/ol.2011.265.
10. Kabalka GW, Smith GT, Dyke JP, Reid WS, Longford CP, Roberts TG, Reddy NK, Buonocore E, Hubner KF: **Evaluation of fluorine-18-BPA-fructose for boron neutron capture treatment planning.** *J Nucl Med* 1997, **38**(11):1762–1767.
11. Zhao S, Kuge Y, Yi M, Zhao Y, Hatano T, Magota K, Nishijima K, Kohanawa M, Tamaki N: **Dynamic 11C-methionine PET analysis has an additional value for differentiating malignant tumors from granulomas: an experimental study using small animal PET.** *Eur J Nucl Med Mol Imaging* 2011, **38**(10):1876–1886. doi:10.1007/s00259-011-1865-2.
12. Kemp BJ, Hruska CB, McFarland AR, Lenox MW, Lowe VJ: **NEMA NU 2-2007 performance measurements of the Siemens Inveon preclinical small animal PET system.** *Phys Med Biol* 2009, **54**(8):2359–2376. doi:10.1088/0031-9155/54/8/007.
13. Pollmann D, Broekaert JAC, Leis F, Tschopel P, Tolg G: **Determination of boron in biological tissues by inductively-coupled plasma optical-emission spectrometry (ICP-OES).** *Fresen J Anal Chem* 1993, **346**(4):441–445. doi:10.1007/Bf00325858.
14. Duffy M, Thomas R: **Benefits of a dual-view ICP-OES for the determination of boron, phosphorus, and sulfur in low alloy steels.** *Atom Spectrosc* 1996, **17**(3):128–132.
15. Yoshimoto M, Kurihara H, Honda N, Kawai K, Ohe K, Fujii H, Itami J, Arai Y: **Predominant contribution of L-type amino acid transporter to 4-borono-2-(18)F-fluoro-phenylalanine uptake in human glioblastoma cells.** *Nucl Med Biol* 2013, **40**(5):625–629. doi:10.1016/j.nucmedbio.2013.02.010.
16. Imahori Y, Ueda S, Ohmori Y, Sakae K, Kusuki T, Kobayashi T, Takagaki M, Ono K, Ido T, Fujii R: **Positron emission tomography-based boron neutron capture therapy using boronophenylalanine for high-grade gliomas: part I.** *Clin Cancer Res* 1998, **4**(8):1825–1832.

17. Wang HE, Liao AH, Deng WP, Chang PF, Chen JC, Chen FD, Liu RS, Lee JS, Hwang JJ: **Evaluation of 4-borono-2-18 F-fluoro-L-phenylalanine-fructose as a probe for boron neutron capture therapy in a glioma-bearing rat model.** *J Nucl Med* 2004, **45**(2):302–308.
18. Yang FY, Chang WY, Li JJ, Wang HE, Chen JC, Chang CW: **Pharmacokinetic analysis and uptake of 18 F-FBPA-Fr after ultrasound-induced blood-brain barrier disruption for potential enhancement of boron delivery for neutron capture therapy.** *J Nucl Med* 2014, **55**(4):616–621. doi:10.2967/jnumed.113.125716.
19. Yang FY, Lin YL, Chou FI, Lin YC, Hsueh Liu YW, Chang LW, Hsieh YL: **Pharmacokinetics of BPA in gliomas with ultrasound induced blood-brain barrier disruption as measured by microdialysis.** *PLoS One* 2014, **9**(6):e100104. doi:10.1371/journal.pone.0100104.
20. Ishiwata K, Shiono M, Kubota K, Yoshino K, Hatazawa J, Ido T, Honda C, Ichihashi M, Mishima Y: **A unique in vivo assessment of 4-[10B]borono-L-phenylalanine in tumour tissues for boron neutron capture therapy of malignant melanomas using positron emission tomography and 4-borono-2-[18 F]fluoro-L-phenylalanine.** *Melanoma Res* 1992, **2**(3):171–179.
21. Chandra S, Kabalka GW, Lorey DR 2nd, Smith DR, Coderre JA: **Imaging of fluorine and boron from fluorinated boronophenylalanine in the same cell at organelle resolution by correlative ion microscopy and confocal laser scanning microscopy.** *Clin Cancer Res* 2002, **8**(8):2675–2683.
22. Kessler RM, Ellis JR Jr, Eden M: **Analysis of emission tomographic scan data: limitations imposed by resolution and background.** *J Comput Assist Tomogr* 1984, **8**(3):514–522.
23. Huang SC: **Anatomy of SUV. Standardized uptake value.** *Nucl Med Biol* 2000, **27**(7):643–646.
24. Olivares M, DeBlois F, Podgorsak EB, Seuntjens JP: **Electron fluence correction factors for various materials in clinical electron beams.** *Med Phys* 2001, **28**(8):1727–1734.
25. Sakata M, Oda K, Toyohara J, Ishii K, Nariai T, Ishiwata K: **Direct comparison of radiation dosimetry of six PET tracers using human whole-body imaging and murine biodistribution studies.** *Ann Nucl Med* 2013, **27**(3):285–296. doi:10.1007/s12149-013-0685-9.
26. Lin YC, Hwang JJ, Wang SJ, Yang BH, Chang CW, Hsiao MC, Chou FI: **Macro- and microdistributions of boron drug for boron neutron capture therapy in an animal model.** *Anticancer Res* 2012, **32**(7):2657–2664.
27. Mishima Y, Imahori Y, Honda C, Hiratsuka J, Ueda S, Ido T: **In vivo diagnosis of human malignant melanoma with positron emission tomography using specific melanoma-seeking 18F-DOPA analogue.** *J Neurooncol* 1997, **33**(1–2):163–169.
28. Imahori Y, Ueda S, Ohmori Y, Sakae K, Kusuki T, Kobayashi T, Takagaki M, Ono K, Ido T, Fujii R: **Positron emission tomography-based boron neutron capture therapy using boronophenylalanine for high-grade gliomas: part II.** *Clin Cancer Res* 1998, **4**(8):1833–1841.
29. Miyashita M, Miyatake S, Imahori Y, Yokoyama K, Kawabata S, Kajimoto Y, Shibata MA, Otsuki Y, Kirihata M, Ono K, Kuroiwa T: **Evaluation of fluoride-labeled boronophenylalanine-PET imaging for the study of radiation effects in patients with glioblastomas.** *J Neurooncol* 2008, **89**(2):239–246. doi:10.1007/s11060-008-9621-6.
30. Kageji T, Mizobuchi Y, Nagahiro S, Nakagawa Y, Kumada H: **Clinical results of boron neutron capture therapy (BNCT) for glioblastoma.** *Appl Radiat Isot* 2011, **69**(12):1823–1825. doi:10.1016/j.apradiso.2011.05.029.
31. Kato I, Ono K, Sakurai Y, Ohmae M, Maruhashi A, Imahori Y, Kirihata M, Nakazawa M, Yura Y: **Effectiveness of BNCT for recurrent head and neck malignancies.** *Appl Radiat Isot* 2004, **61**(5):1069–1073. doi:10.1016/j.apradiso.2004.05.059.
32. Suzuki M, Sakurai Y, Hagiwara S, Masunaga S, Kinashi Y, Nagata K, Maruhashi A, Kudo M, Ono K: **First attempt of boron neutron capture therapy (BNCT) for hepatocellular carcinoma.** *Jpn J Clin Oncol* 2007, **37**(5):376–381. doi:10.1093/jjco/hym039.
33. Altieri S, Bortolussi S, Barth RF, Roveda L, Zonta A: **Thirteenth International Congress on Neutron Capture Therapy.** *Appl Radiat Isot* 2009, **67**(7–8 Suppl):S1–S2. doi:10.1016/j.apradiso.2009.03.009.

doi:10.1186/s13550-014-0070-2
Cite this article as: Hanaoka *et al.*: FBPA PET in boron neutron capture therapy for cancer: prediction of ^{10}B concentration in the tumor and normal tissue in a rat xenograft model. *EJNMMI Research* 2014 **4**:70.

Feasibility studies towards future self-sufficient supply of the ^{99}Mo-^{99m}Tc isotopes with Japanese accelerators

By Kozi NAKAI,[*1,†] Naruto TAKAHASHI,[*2] Jun HATAZAWA,[*3] Atsushi SHINOHARA,[*2] Yoshihiko HAYASHI,[*2] Hayato IKEDA,[*3] Yasukazu KANAI,[*3] Tadashi WATABE,[*3] Mitsuhiro FUKUDA[*1] and Kichiji HATANAKA[*1]

(Communicated by Toshimitsu YAMAZAKI, M.J.A.)

Abstract: In order to establish a self-sufficient supply of ^{99m}Tc, we studied feasibilities to produce its parent nucleus, ^{99}Mo, using Japanese accelerators. The daughter nucleus, ^{99m}Tc, is indispensable for medical diagnosis. ^{99}Mo has so far been imported from abroad, which is separated from fission products generated in nuclear reactors using enriched ^{235}U fuel. We investigated ^{99m}Tc production possibilities based on the following three scenarios: (1) ^{99}Mo production by the (n, 2n) reaction by spallation neutrons at the J-PARC injector, LINAC; (2) ^{99}Mo production by the (p, pn) reaction at $E_p = 50$–80 MeV proton at the RCNP cyclotron; (3) ^{99m}Tc direct production with a 20 MeV proton beam from the PET cyclotron. Among these three scenarios, scenario (1) is for a scheme on a global scale, scenario (2) works in a local area, and both cases take a long time for negotiations. Scenario (3) is attractive because we can use nearly 50 PET cyclotrons in Japan for ^{99m}Tc production. We here consider both the advantages and disadvantages among the three scenarios by taking account of the Japanese accelerator situation.

Keywords: ^{99}Mo-^{99m}Tc, Accelerator production, J-PARC, PET-cyclotron, Tc generator

1. Introduction

The radioisotope ^{99m}Tc has long been used for medical diagnostic imaging with the SPECT (Single Photon Emission Computed Tomography) in many hospitals and medical facilities (as many as 1,200). Throughout the long history of radio-medical applications, various chemicals labeled by ^{99m}Tc radioactive isotopes have been developed for medical examination[1] (*e.g.* blood flow, bone metastasis, etc.; see Table 1).

The isotope supply in Japan is mostly from abroad, which may possibly have catastrophic impacts on medical activities when some difficulties might occur concerning the import of ^{99}Mo isotopes from abroad in the future. In this paper, we discuss the feasibility for the self-sufficient supply of the ^{99m}Tc isotope in Japan.

The short half-life of ^{99m}Tc ($T_{1/2} = 6.02$ hr) makes a convenient delivering system impossible. However, the ^{99m}Tc isotope is generated through the radioactive decay of ^{99}Mo ($T_{1/2} = 66.0$ hr), which can be easily transported over long distances to hospitals.

The ^{99}Mo isotope has been mostly generated in nuclear reactors using highly enriched ^{235}U fuel (HEU). However, presently, the use of HEU tends to be prohibited due to PTBT (Partial Test Ban Treaty, 1963) and NPT (Treaty on the Non-Proliferation of Nuclear Weapons, 1968), so that the only 5 HEU reactors are in operation world-wide. All of them are more than 50 years old, and are now suffering from various problems. Therefore, we are now encountering a serious problem: that the supply of ^{99}Mo isotopes may often become unstable, and that any ^{99}Mo isotope shortage will reach a crisis level in medical diagonosis.[2]

[*1] Research Center for Nuclear Physics, Osaka University, Osaka, Japan.
[*2] Graduate School of Science, Osaka University, Osaka, Japan.
[*3] Graduate School of Medicine, Osaka University, Osaka, Japan.
[†] Correspondence should be addressed: K. Nakai, Research Center for Nuclear Physics, Osaka University, 10-1 Mihogaoka, Ibaraki, Osaka 567-0074, Japan (e-mail: nakai@post.kek.jp).

doi: 10.2183/pjab.90.413

Table 1. ^{99m}Tc Radioactive medicines (from Ref. 1)

Brain	^{99m}Tc-DTPA, $^{99m}TcO_4$, ^{99m}Tc-HMPAO, ^{99m}Tc-ECD
Thyroid gland	$^{99m}TcO_4^-$
Lungs	^{99m}Tc-MAA*, ^{99m}Tc-colloid, ^{99m}Tc-HAS (* added by present authors)
Heart	^{99m}Tc-sestamibi, ^{99m}Tc-tetrofosmin, ^{99m}Tc-pyrophostate, ^{99m}Tc-red blood cell
Vein	^{99m}Tc-MAA
Liver	^{99m}Tc-phytate, ^{99m}Tc-Sn colloid, ^{99m}Tc-HIDA, ^{99m}Tc-PMT
Salivary gland	$^{99m}TcO_4^-$
Meckel diverticle	$^{99m}TcO_4^-$
Gastrointestinal tract	^{99m}Tc-red blood cell
Kidney	^{99m}Tc-DMSA, ^{99m}Tc-MAG3, ^{99m}Tc-DTPA
Testicles	^{99m}Tc-HSA
Placenta	^{99m}Tc-HSA
Spleen	^{99m}Tc-Sn colloid
Bone	^{99m}Tc-MDP, ^{99m}Tc-HMDP
Lymph node	^{99m}Tc-Re colloid, ^{99m}Tc-Sn colloid

Since the present ^{99}Mo production scheme using HEU violates the regulations of PTBT and NPT, we need to develop alternative methods.[3] Together with world-wide efforts, new methods to produce the ^{99}Mo isotopes have been explored and proposed using Japanese accelerator facilities through photonuclear reactions (γ, n),[4] neutron-induced reactions $(n, 2n)$[5] and (n, γ), as well as proton-incident reactions (p, pn) and $(p, 2n)$.

We started feasibility tests in generating neutrons[6] from the high-energy, high-intensity proton beam of the injector LINAC (Linear Accelerator) of J-PARC (Japan-Proton Accelerator Research Complex). In this paper, we report on a series of feasibility-test experiments at the Ring-Cyclotron facility of RCNP (Research Center of Nuclear Physics). While the J-PARC/injector LINAC could provide a 400 MeV, 300 μA beam, a proton beam of 400 MeV, 1 μA is available at the RCNP/Ring-Cyclotron. The latter has been a nice playground to test the basic ideas and various feasibilities because of easier access and convenience for experimental designs. We also studied the possibilities of using lower energy proton beams for ^{99}Mo production as well as ^{99m}Tc direct production by using the AVF (Azimuthally Varying Field) cyclotron.

2. Production of ^{99}Mo isotopes with spallation neutrons

In nuclear reactions using projectiles above 100 MeV/nucleon, the collision speed becomes faster than the nucleon Fermi motion in nuclei, or above the sound velocity of nuclear matter. Therefore, the neutron yield increases dramatically through the spallation process (see Fig. 1). We expect to increase the ^{99}Mo yield via the ^{100}Mo$(n, 2n)^{99}$Mo reaction. For producing medical isotopes, however, the specific activity is an additional factor to optimize the proton energy. We used a 400 MeV proton beam on a heavy-metal target to produce spallation neutrons, so that the ^{99}Mo isotope would be produced via the ^{100}Mo$(n, 2n)$ reaction on a natural Mo target. A heavy-metal Mo, Ta, or W target was used to generate fast neutrons by the (n, xn) reaction. We used the Monte-Carlo program 'PHITS'[7] (Particle and Heavy Ion Transport code System) for designing the experiments. An example of the PHITS simulation for neutron emission from 400 MeV protons on a thick Ta target is shown in Fig. 2. In contrast to the forward-enhanced distribution at low incident energies, lower than 100 MeV, spallation neutrons are emitted sideways. Hence, a cylindrical target configuration is favorable when using neutrons for the ^{100}Mo$(n, 2n)$ reaction. Figure 3 shows a typical spectrum of spallation neutrons. In this figure, the production cross section for the ^{100}Mo$(n, 2n)^{99}$Mo reaction is inserted. The neutron yields decrease monotonically with increasing the neutron energy. Thus, the overlaps between the neutron yields and the ^{100}Mo$(n, 2n)^{99}$Mo cross section is not ideally good. However, there was almost no way to change the neutron spectrum shape. The high-energy proton beam allows us to use a thick target, as long as 15 cm.

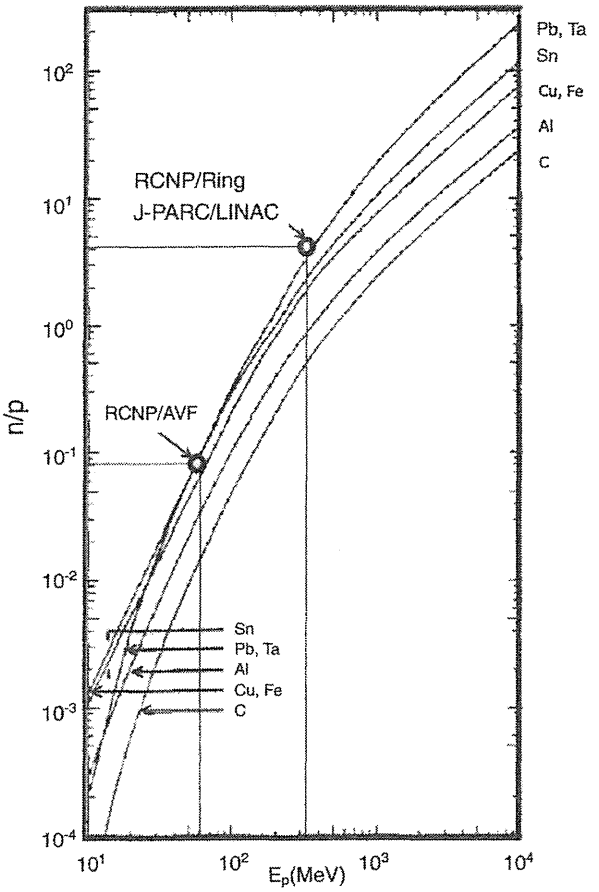

Fig. 1. Number of emitted neutrons per single beam proton (n/p) *vs.* proton energy (E_p), by K. Tesch from Ref. 6.

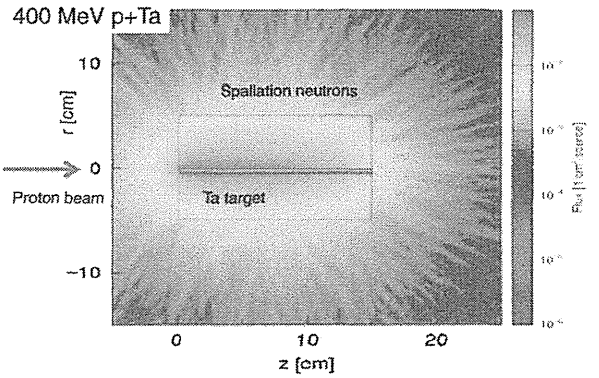

Fig. 2. PHITS simulation of spallation neutron emission from the 400 MeV proton used on a Ta rod of 1.5 cmΦ × 15 cm long. The neutron distribution has cylindrical symmetry around the beam.

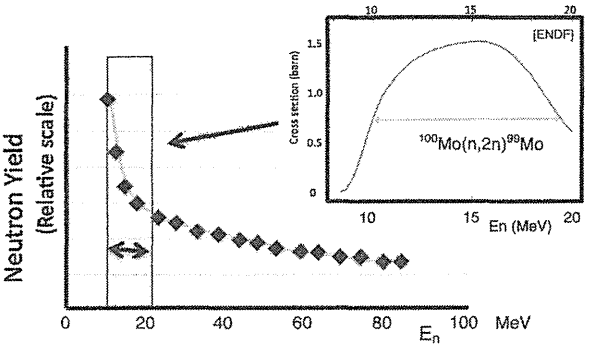

Fig. 3. Spallation neutron spectrum by a 400 MeV proton beam. The ^{100}Mo(n, 2n) cross section (from IAEA (Evaluated Nuclear Data File)) is inserted.

3. Feasibility studies at RCNP for proposing the project at J-PARC

In order to propose a ^{99}Mo-^{99m}Tc production project at J-PARC, we carried out a series of experiments using the 400 MeV proton beam at the Ring cyclotron of RCNP. With the target configuration set to use the cylindrically distributed spallation neutrons, as shown in Fig. 2, experiments were carried out to test ^{99}Mo production. A 400 MeV 35 nA proton beam was incident on a neutron-production target of a natural Mo rod with 15 mm diameter and 150 mm length. The range of 400 MeV protons in a metallic Mo target was calculated to be 128 mm. Neutrons were emitted sideways along the beam axis in the Mo target. For determining the ^{99}Mo production rate, we used natural Mo pellets of 10 mm diameter and 1 mm thickness set along the side of the neutron production target. The irradiation time was 0.5 hr with a beam intensity of 35 nA, *i.e.* 1/10,000 of the J-PARC beam. The next day, after cooling any background activities, γ-ray analyses were performed to determine the yield. The result showed that the ^{99}Mo yield obtained by bombarding the 400 MeV 35 nA proton beam for 0.5 hr on a natural Mo target was at least 10 kBq/g. As shown in Fig. 4, the ^{99}Mo yield expected in the case of J-PARC using the 400 MeV 330 μA proton beam for 10 hr is given by

$$(10\,\mathrm{kBq/g}) \times (330\,\mu\mathrm{A}/35\,\mathrm{nA})(10\,\mathrm{hr}/0.5\,\mathrm{hr}) \sim 2\,\mathrm{GBq/g/10\,hr}$$

If a 500 g natural Mo target is used, we expect to obtain 1 TBq/10 hr. We propose to add this function to the J-PARC/injector-LINAC as a parasite job to be operated independently from the major activities at the 3 GeV and 50 GeV synchrotron rings. As a result, we expect to use nearly 100% of the operating

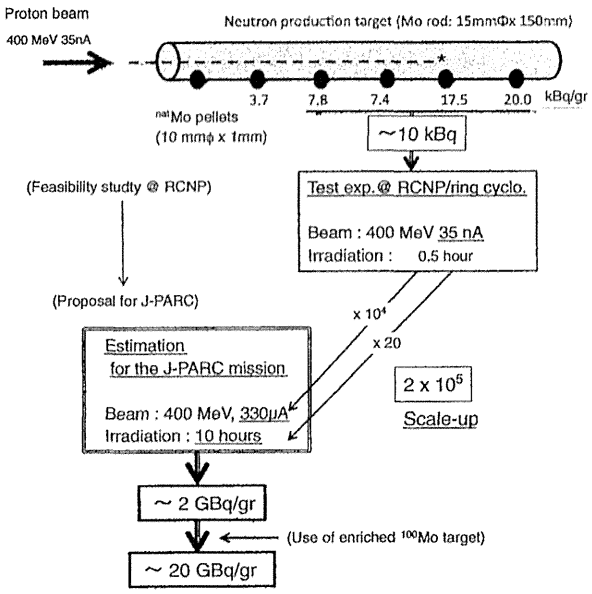

Fig. 4. Results of feasibility test experiments at the RCNP/cyclotron, and an experimental estimation of the ^{99}Mo yields for the proposed J-PARC mission.

time of the injector LINAC. We also expect that J-PARC can operate for 50 weeks over one year, and that the parasitic beam time for 10 hours of irradiation will be scheduled three times a week. Then, the total production time would be (52 week $\times$ 3 $\times$ 10 hr) = 156 $\times$ 10 hr over one year. The total production of ^{99m}Tc would amount to 150 TBq/year. This is about the half of the total amounts of ^{99m}Tc supply (314 TBq in 2013, and 326 TBq in 2012).[8] Note that the yield estimation given here is based on an experiment using natural Mo with a ^{100}Mo natural abundance of 9.63%. Using a highly enriched ^{100}Mo (>90%), ^{99}Mo yield is enhanced by almost a factor of 10, so that the ^{99}Mo yield will reach to cover the total Japanese consumption.

4. Chemical separation and purification of ^{99}Mo-^{99m}Tc for ^{99m}Tc generation

Any chemical handling of ^{99}Mo-^{99m}Tc isotopes at the production target has to be done under an extremely high radiation level with minimum disturbance to the main J-PARC activities.

We use MoO_3 powder as the target material. We can dissolve it by infusing a 4 mol-NaOH solvent after irradiation. Then, the ^{99}Mo isotopes are transferred from the target vessel in the hot area to a carrier of radioactive liquid located outside of the accelerator room.

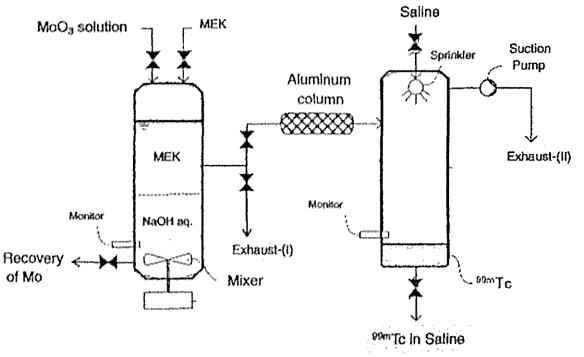

Fig. 5. 'Tc generator' for the chemical separation of ^{99m}Tc from a MoO_3 target. The MoO_3 is desolved in 4nNaOH, and mixed with Methyl ethyl Kepton (MEK) for solvent extraction. Since the first product of extraction contains not only ^{99m}Tc, but also other Tc isopes as well as other elements, it is thrown away from Exhaust-(I). Then, after waiting for about 10 hours for the accumulation of ^{99m}Tc, 2nd and 3rd extractions are repeated to obtain ^{99m}Tc untill the ^{99}Mo in the NaOH aqueous solution decays. In the case an enriched ^{100}Mo is used for ^{99}Mo production, the residue of ^{100}Mo is recovered for later use.

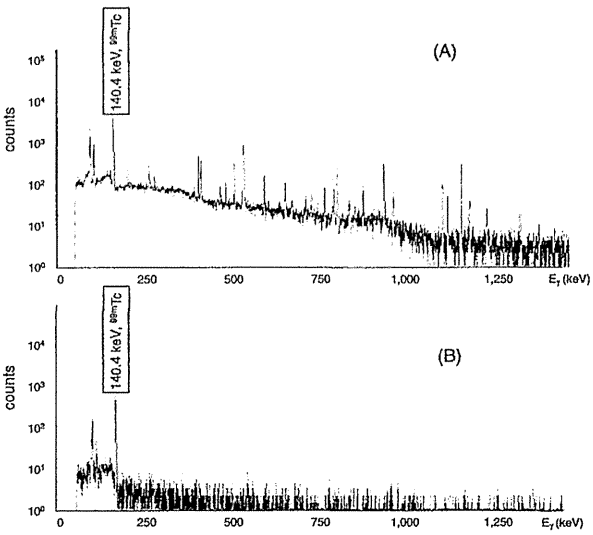

Fig. 6. Performance of chemical separation and purification through the Tc-generator is monitored by γ-ray measurements. Here is an example of γ-ray measurements; (A) is before and (B) is after the chemical process passing through the Tc generator.

We built a new chemical apparatus, named 'Tc generator'[9] (Fig. 5). Figure 6 shows γ-ray spectra obtained both before and after separation through the Tc generator.

A solvent-extraction method with MEK (methyl ethyl keptone) is used for the separation of Tc from Mo. The Tc extracted from Mo was successfully used for taking bone scintigrams.[10),11)]

The (MEK) extraction is carried out in two stages:

(I) A NaOH solution of the Mo target includes ^{99m}Tc together with any impurities as well as other Tc isotopes. Those are extracted in the first extraction after production, and the MEK solution is thrown away.

(II) After waiting for about the half-life necessary for building up ^{99m}Tc in the NaOH solution, a second (MEK) extraction generates ^{99m}Tc in the MEK solution exclusively. Then, the ^{99m}Tc are further purified by passing through an aluminum clomn. This process (II) is repeated several times with intervals of about the half-life of ^{99m}Tc, until the ^{99}Mo is phased out by decay.

In order to examine the performance of the ^{99m}Tc produced by (n, 2n) reaction on a Mo target, we compared the quality of the ^{99m}Tc samples using the present ^{99m}Tc source from Mo target with that using the conventional commercial source separated from fission products.[12] The latter was made by adding commercially available ^{99m}Tc (60 MBq) into a solution of $^{nat}MoO_3$ (40 g) dissolved in NaOH (4 mol in 120 ml). The ^{99m}Tc isotope was extracted with 15 ml of MEK from a solution containing a macro amount of natural Mo. After the evaporation of MEK, the dried sample was dissolved in a few ml of saline, and the solution was purified by passing through a neutral aluminum column to remove any possible residue of Mo. The amounts of impurities, and the extraction efficiency, etc. were measured by using inductivity coupled plasma mass spectroscopy (ICP-MS) and γ-ray spectroscopy with a Ge detector. The yield of ^{99m}Tc was 75–90%. The impurities of Mo and Al were less than 10 ppb.

The labeling efficiency of ^{99m}Tc-MDP was higher than 99%. All of these numbers were found to satisfy the requirement of USP (United Statemacs Pharopeia). The requirement is to keep the impurity at less than 0.01% of the ^{99m}Tc.[18]

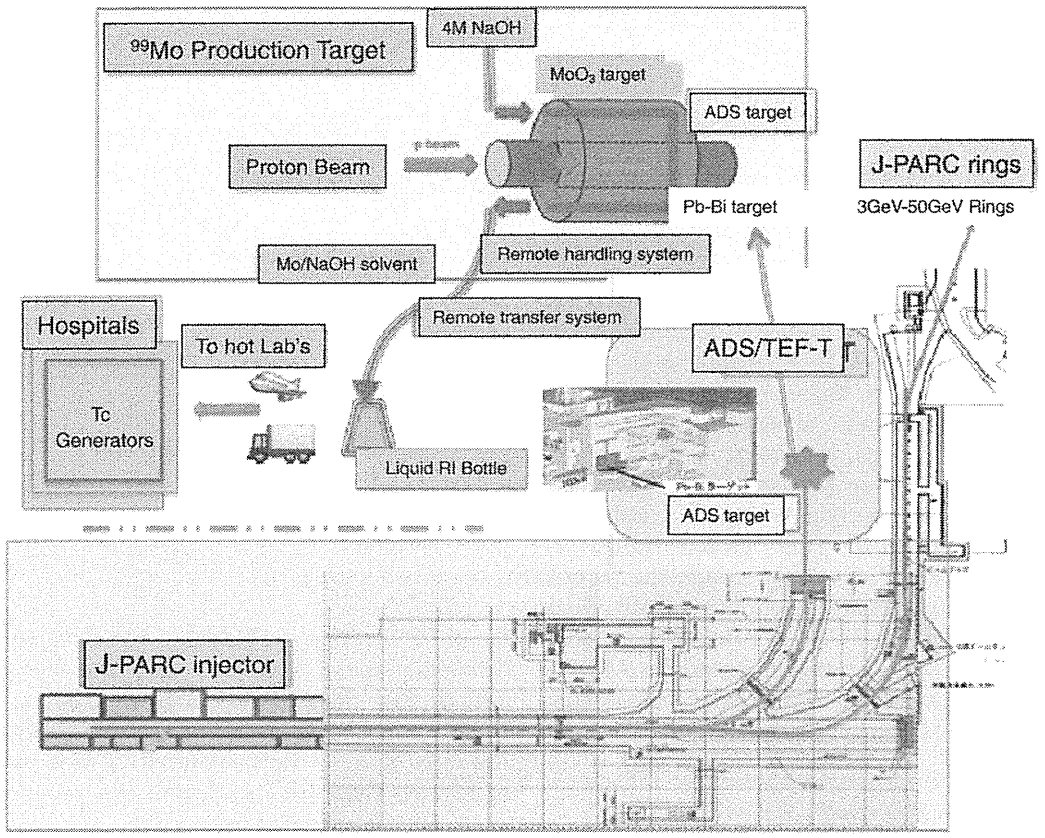

Fig. 7. Proposed layout at the J-PARC injector LINAC. The proton beam line for the ADS/TEF-T project is used so that produced neutrons are used parasitically. The MoO_3 target is used, which is soluble in 4nNaOH, so that any hot isotopes in the solution can be transferred to a liquid RI bottle outside the accelerator room. Chemical process for separation and purification can be done in local hot-laboratories.

5. Design and planning of the neutron source at the J-PARC/TEF-T facility

We propose a parasitic use of spallation neutrons from a target of the 400 MeV proton beam in the ADS/TEF-T (Accelerator-Driven System/Transmutation Experimental Facility-T) beam line with minimum disturbance. Figure 7 shows a preliminary proposal of a layout for ^{99}Mo-^{99m}Tc production, which must be a subject to be improved in practical use. The parasitic use of the beam was emphasized because a radioisotope production for medical use requires a stable supply independently of other activities. Further detailed design work for construction must be completed in collaboration with J-PARC staff members.

6. Test experiments at the RCNP AVF cyclotron to produce ^{99}Mo isotopes through the (p, pn) reaction with a 80 MeV proton beam

When we had completed the feasibility studies discussed in the previous sections (Sections 2 to 4), and had designed the preliminary scheme discussed in Section 5, we learned that the ADS/TEF-T project might take more time than we had expected. We started to explore other possibilities of using a proton beam with the RCNP AVF (Azimuthally Varying Field) cyclotron.

Shown in Fig. 8 is the excitation function of the ^{99}Mo production through the (p, pn) reaction.

We studied the contributions of the background reactions, and concluded that the optimum beam energy would be 50 to 80 MeV. Although the thick target yield increases at higher energy, it is by not more than 100 MeV because of background reactions, such as (p, p2n), (p, p3n), increase.

The 80 MeV 1 μA proton beam from the AVF-cyclotron was used to bombard a Mo pellet of 10 mmφ, 8.6 mm thick (the proton range is 8.55 mm) to test the ^{99}Mo yield through the (p, pn) reaction. The experimentally obtained ^{99}Mo yield was 40 MBq/μA/hour. With a 10 hours bombardment of a 10 μA proton beam, we can produce 4 GBq ^{99}Mo isotopes that are sufficient to satisfy the weekly demand of Osaka University hospital.

7. Test of the direct production of ^{99m}Tc via the Mo(p, 2n) reaction with a 20-MeV proton beam from the RCNP cyclotron

The direct production of ^{99m}Tc isotopes via the ^{100}Mo(p, 2n) reaction was beyond our scope when we started the present project. We thought that the half-life of ^{99m}Tc ($T_{1/2}$ = 6 hours) is too short to make a delivering system to cover a wide area. However, we noticed that about 50 PET cyclotrons (E_p = 18 or 20 MeV) are in operation at various locations in Japan to produce isotopes for PET (see red marks in Fig. 9). Each PET cyclotron can produce ^{99m}Tc isotopes for in-hospital use.

In order to test the feasibility of the method using the 20 MeV PET cyclotron for the direct production of ^{99m}Tc isotopes via the Mo(p, 2n) reaction, we bombarded a 20 MeV 50 nA proton beam on a natural

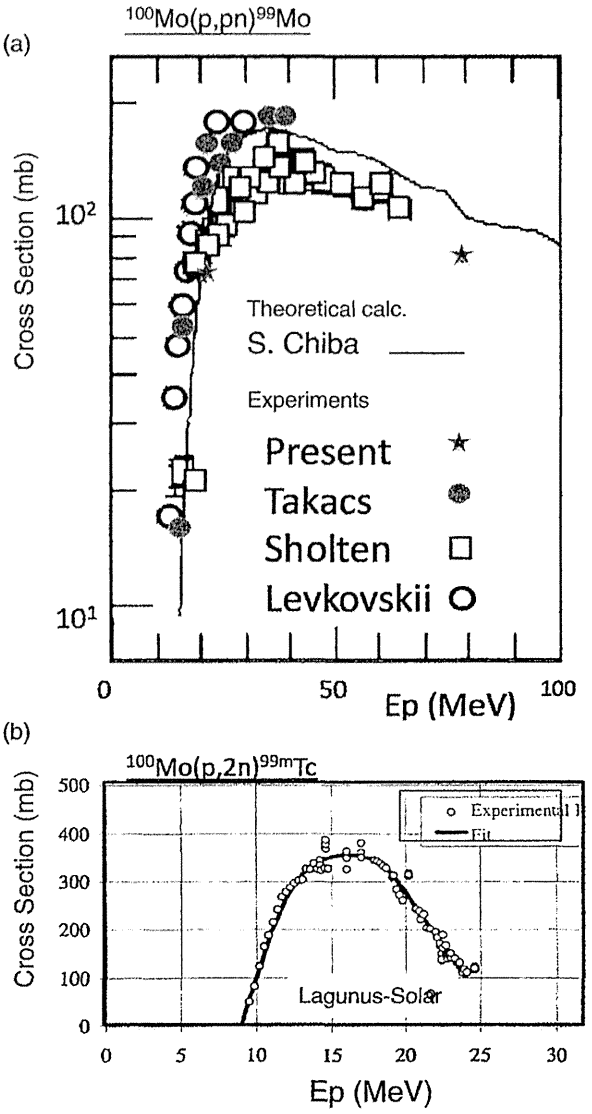

Fig. 8. Excitation functions of (a) ^{100}Mo(p, pn)^{99}Mo, and (b) ^{100}Mo(p, 2n)^{99m}Tc reactions. Experimental data from Refs. 14 to 17 are plotted.

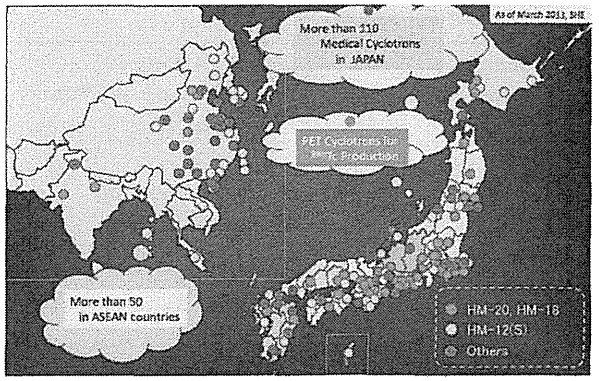

Fig. 9. Distribution of low-energy cyclotrons constructed by Japanese SHI (Sumitomo Heavy Industries). Among them, the red marks indicate those that are usable for the direct generation of ^{99m}Tc.

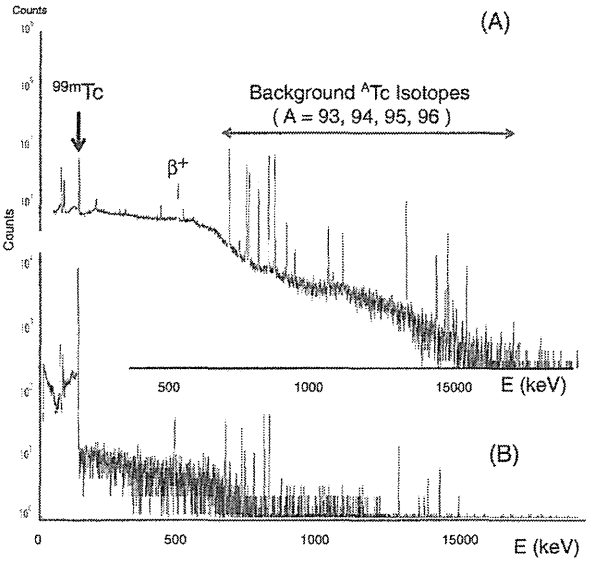

Fig. 10. Gamma-ray spectra from the 20 MeV proton beam on a Mo target, taken 10 hours after EOB. The upper spectrum (A) is with a natural target. The lower one (B) is with a 95% enriched ^{100}Mo target and after the chemical process passing through the 'Tc generator'. All peaks in the spectrum (B) were assigned to be gamma-rays from Tc isotopes.

MoO_3 pellet target having a thickness of 0.4 g/cm^2. Although the irradiation time was only 10 min, we were able to obtain ^{99m}Tc of about 5.6×10^4 Bq, which led us to conclude that the ^{99m}Tc production yield is 21 MBq/μA/hour (at EOB).

The direct production of ^{99m}Tc isotopes through the ^{100}Mo(p, 2n) reaction using a medical cyclotron has been investigated since the early 1970's[13] as an alternative candidate of the HEU nuclear reactors.

Measurements of the excitation function of the (p, 2n) reaction have been reported by three groups.[15)–17)] Although the absolute cross sections are not quite in good agreement, their proton energy dependences are similar, showing a broad peak from 15 to 20 MeV (see Fig. 8(b)).

We compared our data of yield measurements with the calculated yield by integrating their excitation data. Our data were in agreement with a calculation based on data obtained by Scholten *et al.*[15)]

We estimated that by using a 1 μA proton beam on a 96% enriched ^{100}Mo target with a thickness of 0.5 g/cm^2 for 10 hours, the yield of ^{99m}Tc isotopes would be 3.5 GBq. This amount should be sufficient for typical hospitals. Through the test experiment with only 10 minutes of proton bombardment on a natural Mo target, we concluded that PET cyclotrons are useful for direct ^{99m}Tc production. However, the γ-ray spectra showed not only the ^{99m}Tc isotope, but also many γ-rays from other Tc isotopes (Fig. 10). The Tc isotope contaminations were ^{93}Tc ($T_{1/2} = 2.8$ h), ^{94}Tc ($T_{1/2} = 4.9$ h), ^{95}Tc ($T_{1/2} = 20$ h) and ^{96}Tc ($T_{1/2} = 4.3$ d). Those are difficult to separate through chemical processes. Obviously, we need to use highly enriched ^{100}Mo (higher than 99.5%).[18)] In order to reduce the production cost, we started to design a new target system for multiple use of the expensive ^{100}Mo.

8. Summary of feasibility research at RCNP, and concluding remarks

Through the series of RCNP experiments discussed above concerning the feasibility study of the ^{99}Mo-^{99m}Tc production by the J-PARC injector beam, we were able to show that sufficient amounts of ^{99}Mo isotopes could be produced to cover the total Japanese consumption. Through this work, we are convinced that the method of producing ^{99m}Tc isotopes from a Mo target by the accelerator is good despite the fact that the specific activity of ^{99}Mo is very low. It makes a contrast to the method hitherto well established for Mo chemical separation from fission products generated in nuclear reactors using enriched ^{235}U fuel.

Hence, the alternative work would also contribute to reduce the use of enriched ^{235}U fuel.

In Table 2, we summarize our efforts in three scenarios.

We established a Japanese style solution using the world top-level high-power accelerator facility, J-PARC. Through the feasibility study using the

Table 2. Summary of feasible experiments and future prospect

	Scenario(1) [Section-3, 4, 5] Production of ^{99}Mo (for Milking) ^{100}Mo(n, 2n)^{99}Mo with spallation neutron	Scenario(2) [Section-6] Production of ^{99}Mo (for Milking) ^{100}Mo(p, pn)^{99}Mo	Scenario(3) [Section-7] Direct Production of ^{99m}Tc ^{100}Mo(p, 2n)^{99m}Tc
Feasibility studies at RCNP			
Beam	proton 400 MeV, 35 nA	proton 80 MeV, 1 μA	proton; 20 MeV, 50 nA
Target	natural Mo	natural Mo	96% enriched ^{100}Mo
Yield	10 kBq/g/0.5 h	40 MBq/μA/h	21 MBq/μA/h
Proposal for production at any Japanese accelerator			
	Scenario(1)	Scenario(2)	Scenario(3)
Facility	J-PARC, ADC/TEF-T (parasitic use)	Existing cyclotrons	PET cyclotrons
Beam	proton; 400 MeV, 330 μA	(Sendai, Takasaki, Saitama,	proton; 15–20 MeV, 100 μA
Target	natural Mo	Chiba, Osaka, ···)	>99.% enriched ^{100}Mo
Yield	2 GBq/g/10 h = 1 TBq/500 g/10 h = 150 TBq/year (52week:3times/week)	*[Local support for emergency]* *e.g. Osaka-U. Hospital*	3.5 GBq/μA/10 h = 350 GBq/100 μA/10 h
Target	>90% enriched ^{100}Mo	*natural Mo*	
Yield	1,500 TBq/year	*~4 GBq/10 μA/10 h*	
Demand	[Japanese consumption ~ 350 TBq/year]	*[3.7 GBq/week]*	

400 MeV proton beam from the RCNP/RING-cyclotron, it has been shown that a sufficient amount of ^{99}Mo can be produced at the J-PARC TEF-T beam line.

We realized, however, that even though the total amount of the isotope production is sufficient, there still remain serious difficulties. For instance, after we achieved full confidence about ^{99}Mo-^{99m}Tc production using the J-PARC, a serious question has arisen. The question is: "what can we do during the period while the J-PARC is not in operation?" The most important factor in serving such medical radioactive isotopes, like ^{99}Mo, is stable supply. The solution for the requirement to assure stable supply of isotopes is to have a plural number of production sources.

Among the three scenarios in Table 2, while scenario (1) is a scheme of global scope, scenario (3) would work in domestic hospitals.

^{99}Mo isotope production at the J-PARC (Scenario (1)). In order to respond to the world-wide crisis of the ^{99}Mo isotope supply with accelerators in lieu of nuclear reactors, the high-energy, high-intensity accelerator, J-PARC is the most suitable facility. Indeed, we have shown through experiments at RCNP that a sufficient amount of ^{99}Mo isotope production is feasible at J-PARC using the spallation neutrons. Since we are considering to use the ADS/TEF-T beam line, we have to wait a few more years for the TEF-T facility.

^{99m}Tc direct production at the PET cyclotrons (Scenario (3)). We learned that in Japan there exist 50 PET cyclotrons that cover the best energy for the direct production of the ^{99m}Tc isotope. A series of test experiments at the RCNP cyclotron have shown the feasibility of direct production. We thought this to be most promising and practical, being an exclusive medical project.

We found, however, the following two weak points: (1) An expensive enriched ^{100}Mo target has to be used; otherwise, contaminations due to other Tc isotopes can not be separated. (2) In the case of an emergency, the production of the ^{99m}Tc isotope takes at least a couple of hours for preparation before an examination. Therefore, the conventional Mo generation must be kept, and we must continue efforts towards a self-sufficient supply of the ^{99}Mo isotopes in parallel.

The ^{99}Mo isotope production network (Scenario (2)). As mentioned in Section 6, beside J-PARC, we have powerful cyclotrons that accelerate proton beams with an intensity of 100 to 300 μA, and with an energy of up to 70 or 80 MeV. Those cyclotrons in Japan are all constructed by SHI (Sumitomo Heavy Industry) at Sendai (CYRIC/Tohoku U.), Takasaki (JAEA), and Chiba (NIRS). If these machines provide 200 μA beam on 90% enriched ^{100}Mo targets for 10 hours, each machine could produce 400 GBq ^{99}Mo. Total amounts of

$3 \times 0.4 = 1.2$ TBq of ^{99}Mo/day are expected to be produced. If the production could be continued for 54 weeks in total during each year, the yield of 65 TBq ^{99}Mo isotopes is available. This amount is sufficient to cover the ^{99}Tc direct production program at the PET cyclotrons (discussed in Scenario (3)) to establish a self-sufficient supply. We will have to start negotiation with the nuclear physics community.

The Tc-generator. In all of the cases using the (n, 2n), (n, γ), (γ, n), (p, pn) and (p, 2n) reactions on a Mo target, the 'Tc generator' discussed in Section 4 is useful for the separation of ^{99m}Tc from ^{99}Mo isotopes produced with very low specific activities. The new method has overcome the difficulty in the chemical separation of the ^{99}Mo radioactive isotopes. It is also contributing greatly to stop using the highly enriched ^{235}U (HEU).

Acknowledgement

The present work was supported by the Research Center for Nuclear Physics (RCNP) Osaka University. We are indebted to Director T. Nakano and supporting staffs of RCNP. We owe thanks to Dr. M. Fujiwara for his careful and critical reading of the present paper. We express many thanks to Dr. I. Tanihata, for continuous encouragement and much advice. This work was supported by a Grant-in-Aid Scientific Research (A) (Number 24241030).

References

1) Kozuka, T., Inamura, K., Doi, K. and Sumita, I. (eds.) (2012) Text book of Clinico-Radiological Technology. Vol. 13, Nankodo, Tokyo, Japan.
2) van Noorden, R. (2013) The medical testing crisis. Nature **504**, 202–204.
3) Lyra, M., Charalambatou, P., Roussou, E., Fytros, S. and Baka, I. (2011) Alternative production methods to face global molybdenum-99 supply shortage. Helenic J. Nucl. Med. **14**, 49–55.
4) Ejiri, H., Shima, T., Miyamoto, S., Horikawa, K., Kitagawa, Y., Asano, Y., Date, S. and Ohashi, Y. (2011) Resonant Photonuclear Reactions for Isotope Transmutation. J. Phys. Soc. Jpn. **80**, 094202-1.
5) Nagai, Y. and Hatsukawa, Y. (2009) Production of ^{99}Mo for nuclear medicine by ^{100}Mo(n, 2n)^{99}Mo. J. Phys. Soc. Jpn. **78**, 033201.
6) Tesch, K. (1985) A simple estimation of the lateral shielding for proton accelerators in energy range 50 to 1000 MeV. Radiat. Prot. Dosimetry **11**, 165–172.
7) Niita, K., Matsuda, N., Hashimoto, S., Iwamoto, Y., Sato, T., Nakashima, H., Sakamoto, Y., Fukahori, T., Chiba, S., Iwase, H. and Sihver, L. Particle and Heavy Ion Transport code system (PHITS).
8) Japan Radioisotope Association (2014) Amounts of ^{99m}Tc Injection in Fiscal 2009–2013, Statistics on the Distribution of Radioisotopes in Japan (2014).
9) Takahashi, N. Patent 2012-224859 (domestic) and Patent 2014/057900A1 (international).
10) Takahashi, N., Nakai, K., Shinohara, A., Hatazawa, J., Nakamura, M., Fukuda, M., Hatanaka, K., Morikawa, Y., Kobayashi, M. and Yamamoto, S. (2012) Production of ^{99}Mo-^{99m}Tc by using spallation neutron. SNM 2012 Annual Meeting, Miami.
11) Ikeda, H., Hayashi, Y., Takahashi, N., Shinohara, A., Watabe, T., Horitsugu, G., Kanai, Y., Watanabe, H. and Hatazawa, J. (2013) Purification of Tc-99m from Macro Mo Target by Solvent Extraction for Nuclear Medicine. SNM 2013 Annual Meeting, Vancouver.
12) Hayashi, Y., Takahashi, N., Nakai, K., Ikeda, H., Horitsugu, T., Watabe, T., Kanai, Y., Shimosegawa, E., Miyake, Y., Hatazawa, J., Fukuda, M., Hatanaka, K., Takamiya, K., Yamamoto, S., Kasamatsu, Y. and Shinohara, A. (2013) Production of ^{99}Mo-^{99m}Tc by using spallation neutron. APSORC'13-5th Asia-Pacific Symposium on Radiochemistry, Kanazawa.
13) Beaver, J.E. and Hupf, H.B. (1971) Production of ^{99m}Tc on amedical cyclotron: a feasibility study. J. Nucl. Med. **12**, 739–741.
14) Takács, S., Szűcs, Z., Tárkányi, F., Hermanne, A. and Sonck, M. (2003) Evaluation of proton induced reactions on 100Mo: New cross sections for production of ^{99m}Tc and 99Mo. J. Radioanal. Nucl. Chem. **257**, 195–201.
15) Sholten, B., Lambrecht, R.M., Cogneauc, M., Ruizd, H.V. and Qaim, S.M. (1999) Excitation functions for the cyclotron production of ^{99m}Tc and ^{99}Mo. Appl. Radiat. Isot. **51**, 69–80.
16) Levkovskii, V.N. (1991) Activation cross section of nuclides with average masses (A = 40–100) by protons and alpha particles with average energies (E = 10–50 MeV). Inter Vesi, Moscow, Russia, p. 155.
17) Laguna-Solar, M.C. (1997) Accelerator Production of ^{99m}Tc with Proton Beams and Enriched ^{100}Mo Targets. IAEA Organized Meeting, Faure South Africa, IAEA-TECDOC1065.
18) Guérin, B., Tremblay, S., Rodrigue, S., Rousseau, J.A., Dumulon-Perreault, V., Lecomte, R., van Lier, J.E., Zyuzin, A. and van Lier, E.J. (2010) Cyclotron production of ^{99m}Tc: An approach to the medical isotope crisis. J. Nucl. Med. **51**, 13N–16N.

(Received Aug. 5, 2014; accepted Oct. 11, 2014)

PLOS | ONE

Distribution of Intravenously Administered Acetylcholinesterase Inhibitor and Acetylcholinesterase Activity in the Adrenal Gland: ^{11}C-Donepezil PET Study in the Normal Rat

Tadashi Watabe[1,2]*, Sadahiro Naka[3], Hayato Ikeda[4], Genki Horitsugi[4], Yasukazu Kanai[1,2], Kayako Isohashi[2,4], Mana Ishibashi[4], Hiroki Kato[2,4], Eku Shimosegawa[2,4], Hiroshi Watabe[1,2¤], Jun Hatazawa[2,4,5]

1 Department of Molecular Imaging in Medicine, Osaka University Graduate School of Medicine, Suita, Osaka, Japan, **2** PET molecular Imaging Center, Osaka University Graduate School of Medicine, Suita, Osaka, Japan, **3** Osaka University Hospital, Suita, Osaka, Japan, **4** Department of Nuclear Medicine and Tracer Kinetics, Osaka University Graduate School of Medicine, Suita, Osaka, Japan, **5** Immunology Frontier Research Center, Osaka University, Suita, Osaka, Japan

Abstract

Purpose: Acetylcholinesterase (AChE) inhibitors have been used for patients with Alzheimer's disease. However, its pharmacokinetics in non-target organs other than the brain has not been clarified yet. The purpose of this study was to evaluate the relationship between the whole-body distribution of intravenously administered ^{11}C-Donepezil (DNP) and the AChE activity in the normal rat, with special focus on the adrenal glands.

Methods: The distribution of ^{11}C-DNP was investigated by PET/CT in 6 normal male Wistar rats (8 weeks old, body weight = 220±8.9 g). A 30-min dynamic scan was started simultaneously with an intravenous bolus injection of ^{11}C-DNP (45.0±10.7 MBq). The whole-body distribution of the ^{11}C-DNP PET was evaluated based on the Vt (total distribution volume) by Logan-plot analysis. A fluorometric assay was performed to quantify the AChE activity in homogenized tissue solutions of the major organs.

Results: The PET analysis using Vt showed that the adrenal glands had the 2nd highest level of ^{11}C-DNP in the body (following the liver) (13.33±1.08 and 19.43±1.29 ml/cm^3, respectively), indicating that the distribution of ^{11}C-DNP was the highest in the adrenal glands, except for that in the excretory organs. The AChE activity was the third highest in the adrenal glands (following the small intestine and the stomach) (24.9±1.6, 83.1±3.0, and 38.5±8.1 mU/mg, respectively), indicating high activity of AChE in the adrenal glands.

Conclusions: We demonstrated the whole-body distribution of ^{11}C-DNP by PET and the AChE activity in the major organs by fluorometric assay in the normal rat. High accumulation of ^{11}C-DNP was observed in the adrenal glands, which suggested the risk of enhanced cholinergic synaptic transmission by the use of AChE inhibitors.

Citation: Watabe T, Naka S, Ikeda H, Horitsugi G, Kanai Y, et al. (2014) Distribution of Intravenously Administered Acetylcholinesterase Inhibitor and Acetylcholinesterase Activity in the Adrenal Gland: ^{11}C-Donepezil PET Study in the Normal Rat. PLoS ONE 9(9): e107427. doi:10.1371/journal.pone.0107427

Editor: Israel Silman, Weizmann Institute of Science, Israel

Received June 4, 2014; **Accepted** August 10, 2014; **Published** September 16, 2014

Data Availability: The authors confirm that all data underlying the findings are fully available without restriction. Data are available from the MIbase system in Osaka University Graduate School of Medicine for researchers who meet the criteria for access to confidential data. Contact address: PET Molecular Imaging Center (info@pet.med.osaka-u.ac.jp).

Funding: This study was supported by KAKENHI Grant-in-Aid for Scientific Research (S) (No. 24229008), Grant-in-Aid for Young Scientists (B) (No. 25861099), and Molecular Imaging Research Strategic Program, a grant (No. 10048012) from Ministry of Education, Culture, Sports, Science and Technology. The funders had no role in study design, data collection and analysis, decision to publish, or preparation of the manuscript.

Competing Interests: The authors have declared that no competing interests exist.

* Email: twatabe@mi.med.osaka-u.ac.jp

¤ Current address: Cyclotron and Radioisotope Center, Tohoku University, Sendai, Miyagi, Japan

Introduction

Acetylcholinesterase (AChE) is one of the most crucial enzymes in the nervous system. AChE is a tetrameric serine hydrolase that rapidly degrades the neurotransmitter acetylcholine (ACh) into choline and acetate [1]. It is mainly found at the neuromuscular junctions and cholinergic synapses in the central nervous system, where its activity serves to terminate synaptic transmission. Progressive loss of cholinergic neurons is observed in Alzheimer's disease (AD) patients with severe memory loss and impairment of cognitive function [2], and AChE inhibitors have been used for such patients to protect against the reduction of acetylcholine in the synapses and to enhance cholinergic activity in the affected regions of the brain [3]. Recently, various types of AChE